

Feature Extraction of Tree-Related High Impedance Faults as a Source of Electromagnetic Interference around Medium Voltage Power Lines' Corridors

Nooshin Bahador, Farhad Namdari*, and Hamid Reza Matinfar

Abstract—One of the faults in medium voltage (MV) overhead power line is a high impedance fault (HIF) owing to low-current discharge to a tree (THIF). This type of fault generates signals in wide frequency bandwidth which may lead to electromagnetic interference (EMI) with neighboring devices and consequently results in degradation in the performance of nearby systems. This problem becomes more critical when MV power lines path is located in a wooded area in which there will be frequent transient conflicts between trees and power lines especially in the windy conditions. Given the importance of this issue, the ability of THIF to generate EMI is first demonstrated in this paper. Thereafter, a hybrid technique based on combination of quantile regression (QR) and empirical mode decomposition (EMD) is proposed to perform a feature extraction from THIF signals. By comparing the QR results of different samples of THIF signal with other similar signals, the validation of proposed method is depicted. In summary, the original contributions of current research include 1) assessing EMI due to THIFs, 2) using EMD in pre-processing of THIFs signals and extracting their main components, 3) recommending QR for the feature definition of THIF.

1. INTRODUCTION

Infrastructure that exists adjacent to medium voltage power lines may be exposed to the electromagnetic field generated by the hidden faults as high impedance faults.

HIFs are low-current signals composed of the superposition of continuous signal, transient, and random disturbances which make them difficult to detect. THIFs are one complex type which occurs when power lines transiently come in contact with live trees. In some cases, the amplitude of THIF is extremely small which makes it very unlikely to be detected by conventional protective devices (e.g., over current relays) and also could not lead to outage. The importance of these low-current THIFs becomes evident when it was found that they are the sources of EMI with nearby systems. This EMI which may lead to the malfunctioning of nearby electronic equipment has become a serious problem given that military and digital communication systems now contain a large number of sensitive devices that are very susceptible to EMI. This EMI may result in critical data loss and degradation in the performance of nearby systems [1–4]. A way to combat this type of EMI in power networks is through the use of EMI cable-shielding for overhead power lines. But most of the MV power lines are bare conductors, and there is no possibility to use shielding for EMI prevention. To achieve reliable and secure electrical power grid, traditional power lines should be replaced with the next generation power lines with special coating which not only solves EMI problem but also prevent power lines from overheating and increases their current carrying [5].

Received 28 February 2017, Accepted 20 April 2017, Scheduled 6 May 2017

* Corresponding author: Farhad Namdari (namdari.f@lu.ac.ir).

The authors are with the Lorestan University, Iran.

Regarding the importance of measurement and specific features definition of EMI sources, some researchers have employed statistical approaches to EMI evaluation of the interference signal in the time-domain [6–8]. There have also been several studies which employed identification method for EMI sources based on the signal processing techniques [9]. But none of these researches have worked on EMI owing to the HIFs. Moreover, HIFs occur on various materials such as live tree, asphalt or concrete, and each results in different features such as fault current amplitude [10, 11]. So, it is not applicable to use same detection techniques for all types of HIF. Given the importance of this issue, none of the researches extracted feature for live tree-power lines conflict and mostly focused on the broken conductor-based HIF, whereas, tree-power lines conflicts have a large contribution from HIFs.

The most common signature of HIFs is being accompanied by the arc [12]. However, the natures of arcs in different HIFs are not similar. For example, in the case of a broken conductor-based HIF, there is an arc with length in the range of centimeter. On the other hand, the length of arc in THIF hardly reaches a span of over millimeter scale, especially in the case of a tree with high water content.

Despite the differences between various types of HIFs, some similarities can also be seen. For example, positive and negative half cycles of current of all HIFs are different in peak value and shape [13]. The characteristic of all HIFs is also nonlinear [14]. The current magnitude also gradually increases until it attains and maintains a constant level for several cycles [15]. But it should be noted that the speed of increase and the number of cycles to reach threshold are different for various HIFs.

Considering the differences between various types of HIFs, it is important to separately address each type of HIF. In other words, there should be distinct criteria for detecting each type of HIF.

About 40% of all feature extraction methods for the HIFs have been wavelet-based techniques [16, 17]. The wavelet-based methods have also been used in most of the signal decomposition techniques that provide further possibilities to EMI evaluation. However, when a signal is transferred to a new domain such as wavelet domain, some characteristics of the original signal will be lost and cannot be effectively evaluated. This is because the decomposed functions of a signal in wavelet domain are not of the same length as the original signal. For this reason, varying frequency in time may not be preserved. That is why the data may be lost in the wavelet domain. These techniques (Wavelet-based technique) have low ability for feature extraction and are so dependent on types of mother wavelet. On the other hand, a technique as EMD does not have such problems and keeps signals in their own domain. Therefore, EMD is used as an applicable tool for feature extraction of THIFs in this paper. The basis of the EMD is evaluation of local oscillations in the signal. This method studies the trend of variations in the signal between two sequential local extrema so that the details and features of original signal are extracted [18, 19].

Therefore, for all the reasons mentioned above, the aim of this paper is first to prove the ability of THIF in generating electromagnetic noise, and then to study a new hybrid method for identifying THIF as an EMI source. In the proposed method, the specific features of THIF signals are extracted using the combination of signal decomposition technique and QR method.

The rest of this paper is organized as follows. Section 2 summarizes the results obtained from the on-site measurements. The basis of EMI assessment of THIF is discussed in Section 3. Section 4 presents the core algorithm for feature extraction of THIF. The results and findings are also interpreted and described in Section 5. The final conclusions drawn in the last section.

2. MEASUREMENT OF THIF SIGNAL

To collect data for THIF, a series of experiments were carried out on live trees under 20 kV power lines in Hamedan, Iran. To conduct the test, a 20 kV single core copper conductor XLPE insulated power cable was connected to the power line and providing connection to tree in order to simulate a HIF [20] (Fig. 1). As the minimum leakage current in this condition (during THIF in MV network) was in the milliamper regime, to accurately measure the total leakage flowing to the intended connection, current probe of power analyzer with resolution of 0.001 mA (Model Prova 6830A+6801) was closed around the cable. The fault's current waveform of tree was captured by using a power analyzer that provides a high sampling rate of 1024 samples/cycle. Stored data were also downloaded using a laptop.

Given that the tree species that could be tested were numerous, trees were classified into families with similar vascular structure. Vascular structures were considered in the sense that the wall thickness

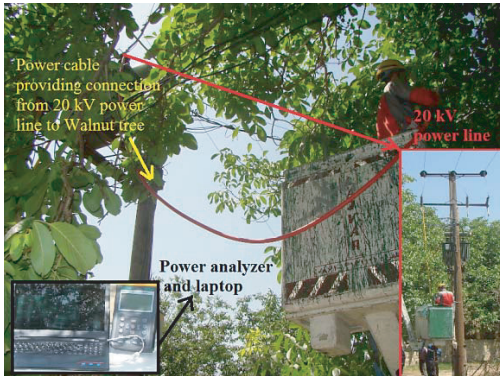


Figure 1. Test configuration for HIF on live Walnut tree.

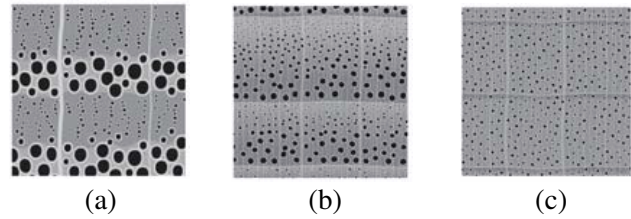


Figure 2. Vascular structure types of broad-leaf trees [21]. (a) Ring porous. (b) Semi-ring porous. (c) Diffuse porous.

Table 1. Broad-leaf trees classification according to vascular structure [22].

Semi-ring Porous	Ring Porous Species	Diffuse Porous
Juglans (Walnut)	Quercus (Oak)	Fagus (Beech)
-	Fraxinus excelsior (Ash)	Acer (Maple)
-	Morus Alba	Populus
-	Ulmus (Elm)	Platanus
-	Zelkova	Salix (Willows)
-	White Acacia	Cherry

Table 2. Broad-leaf species properties according to vascular structure [23].

Ring Porous Species		Diffuse Porous Species		Semi-ring Porous Species	
Spring	Summer	Spring	Summer	Spring	Summer
Large vessels	Tiny vessels	Tiny vessels	Tiny vessels	Medium vessels	Medium vessels
with thin walls	with thick walls	with thick walls	with thick walls	with moderately thick walls	with moderately thick walls

and diameter of vessels, and in other words the electrolyte content of vessels, have direct impact on electrical conductivity (EC) of tree. Therefore, it was just sufficient to perform experiments on one species from each family.

As depicted in Fig. 2, vascular structures of broad-leaf trees are classified into three groups; ring porous, semi-ring porous and diffuse porous. The classification of different trees according to these groups is given in Table 1. The wood of these three groups itself is divided into two categories; spring wood which is formed during spring, and summer wood which is formed during summer or autumn (Table 2).

Water conductivity rate would be higher with increasing water conducting elements size. Because of vascular elements with larger diameter in ring porous species during spring, more water is transferred, and as a result, their moisture content would be more. The EC of each of these types entirely depends on their water content (sap content). So the larger vessels with thinner walls provide more EC.

For the purpose of THIF test, one species from each group (Ash, Walnut and Cherry tree) was

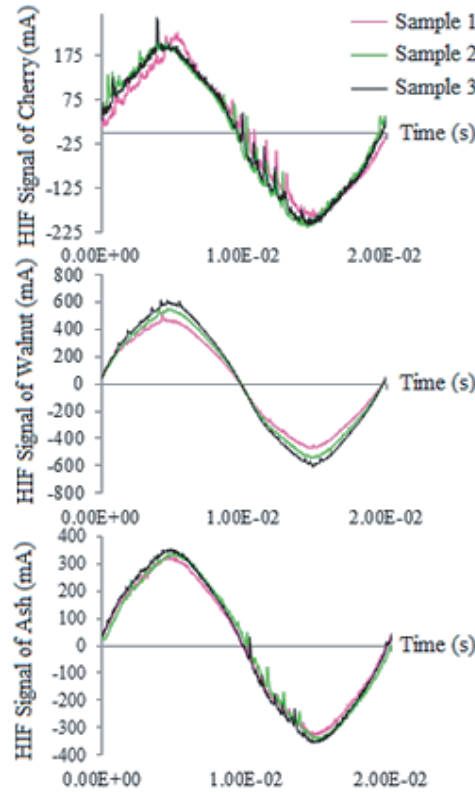


Figure 3. HIF signals of tested trees.

used for the study. Thereafter, three samples of each of the species were selected for the experiment. The fault current waveforms obtained from THIF tests on MV power lines during summer are shown in Fig. 3. The results are as previously hypothesized. The walnut tree is a more conductive tree and have more fault current during summer due to vascular elements with medium diameter. Ash and cherry trees have lower fault current as they have tiny vessels with thick walls during summer. Moreover, as ash and cherry trees have lower water content, their discharge pulses have higher values which is quite obvious in Fig. 3. The divergence of fault current waveforms from sinusoidal form shows nonlinear dependence of fault current on conductor voltage. Positive and negative half cycles are also different in peak value.

3. EMI ASSESSMENT

Evaluation of the emitted magnetic fields by THIF is very essential in EMI assessment. The aim of this section is to model tree-power line conflict and its emitted magnetic field using finite element method (FEM). Fig. 4 shows the modeled structure of THIF. In modeled structure, tree trunk is assumed to be a truncated cone. Trunk diameter at a distance of 100 cm from the ground is about 28.5 cm and near power line is 3 cm. Vertical distance between ground and conductor is 10.8 m.

A 1-km-diameter cylinder is defined around the model (Fig. 5), and the tangential vector magnetic potential is forced to be zero on the lateral surface of defined cylinder. This allows us to ignore scattering fluxes that are closed via the air gap on the external boundary of the computational region by specifying magnetic isolation condition. A 20 kV voltage is applied to the conductor, and measured HIF current (HIF signal of cherry tree) is applied to the electrolyte solution (brine content of vessels) flowing along tree trunk. The ground voltage is also assumed to be zero.

For evaluation of EMI signals generated by cherry-related HIF with nearby systems (e.g., telecommunications equipment), the emission from the THIF in terms of magnetic field is calculated using FEM (Fig. 6) and compared with a standard emission limit in a given frequency (Table 3). As

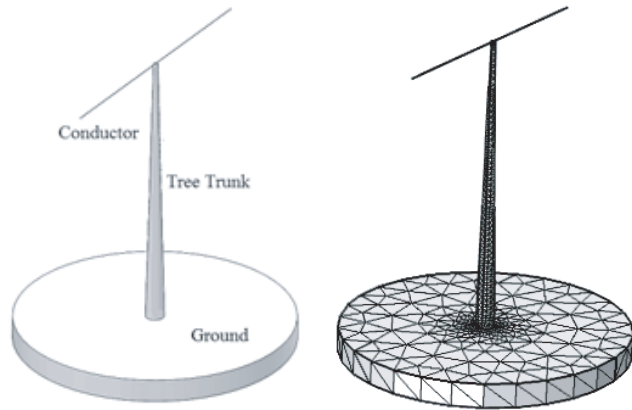


Figure 4. Modeled structure of tree-related HIF.

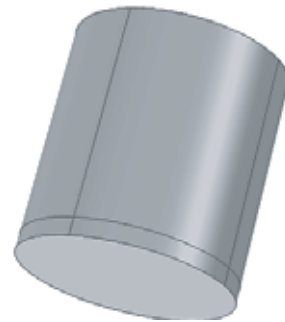


Figure 5. Defined cylinder around model for assuming boundary conditions.

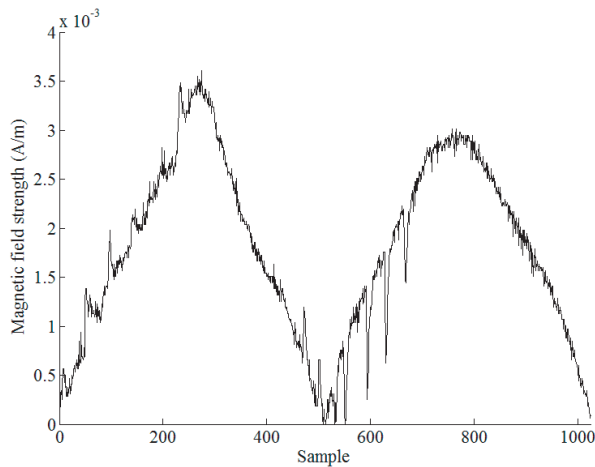


Figure 6. Magnetic field strength amplitude generated by HIF current related to cherry tree at a distance of 10 m.

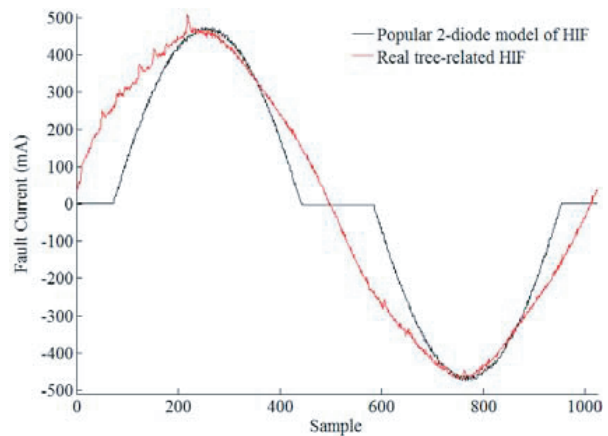


Figure 7. Comparison between current waveform of popular HIF model and real live tree-related HIF.

Table 3. Comparison between OBE unwanted emissions limit and radiated emission due to THIF [24].

Frequency [MHz]	Measurement distance [m]	Peak value [dB μ A/m]	
		Radiated emission limit in ETSI EN 302 608 standard	Radiated emission due to THIF
0.009	10	44	92.932
0.150	10	54	73.256
30	10	4	10.532

shown in Table 3, emissions from the THIF greatly exceed the standard emission limit in high frequency (HF) band.

4. DIFFERENTIATION BETWEEN LIVE THIF AND OTHER TYPES OF HIF

This section differentiates THIF from other types of HIF in terms of physical shape and HF components. The model, selected from a set of candidate models in order to undertake a detailed comparison, was

the well-known HIF model consisting of two antiparallel diodes which had been used in most of the conventional detection methods.

4.1. Differentiation in Terms of Physical Shape

As shown in Fig. 7, for the popular 2-diode HIF model, the fault current waveform is clipped at a specific value due to the forward voltage drop of the diode. But in live THIF signal, no clipping is observed on the waveform.

4.2. Differentiation in Terms of High Frequency Components

HF information contained within signal is what can distinguish live THIF from other HIFs. Therefore, in order to differentiate live THIFs, their HF information should be evaluated. For this purpose, HF information contained within measured live THIF signals was extracted using EMD. The first to fourth Intrinsic mode functions (IMFs) obtained from decomposition were chosen for evaluation. As clear in Fig. 8, none of the functions related to both live THIF and 2-diode HIF have the same distribution. Pulse peak values are also not the same, and there is no apparent relationship between them.

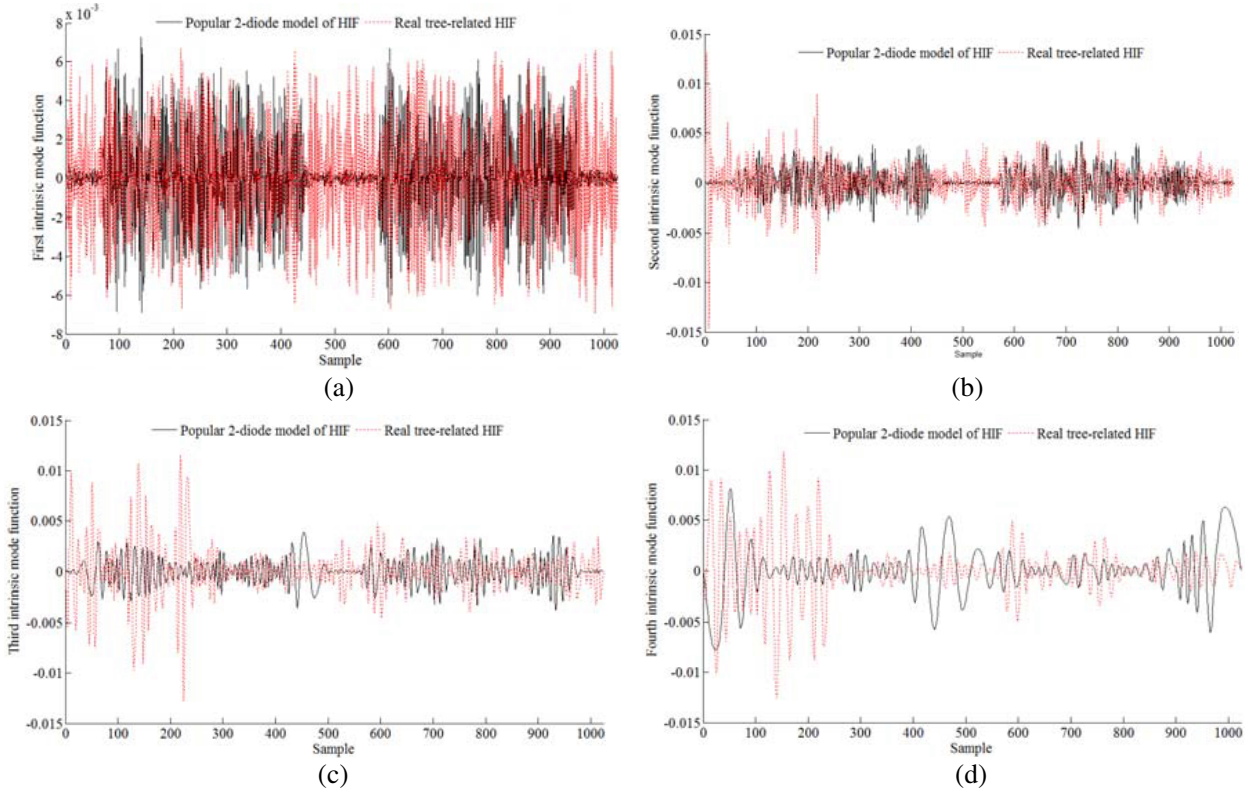


Figure 8. Signal decomposition of both live THIF and 2-diode HIF into their intrinsic mode functions. (a) First intrinsic mode function. (b) Second intrinsic mode function. (c) Third intrinsic mode function. (d) Fourth intrinsic mode function.

5. FEATURE EXTRACTION OF THIF AS AN EMI SOURCE

As previously mentioned, HF information contained within signals is what can distinguish THIFs from other similar events. So, in order to characterize THIFs, their HF information should be evaluated to find a feature. For this purpose, high-frequency information contained within measured HIF signals

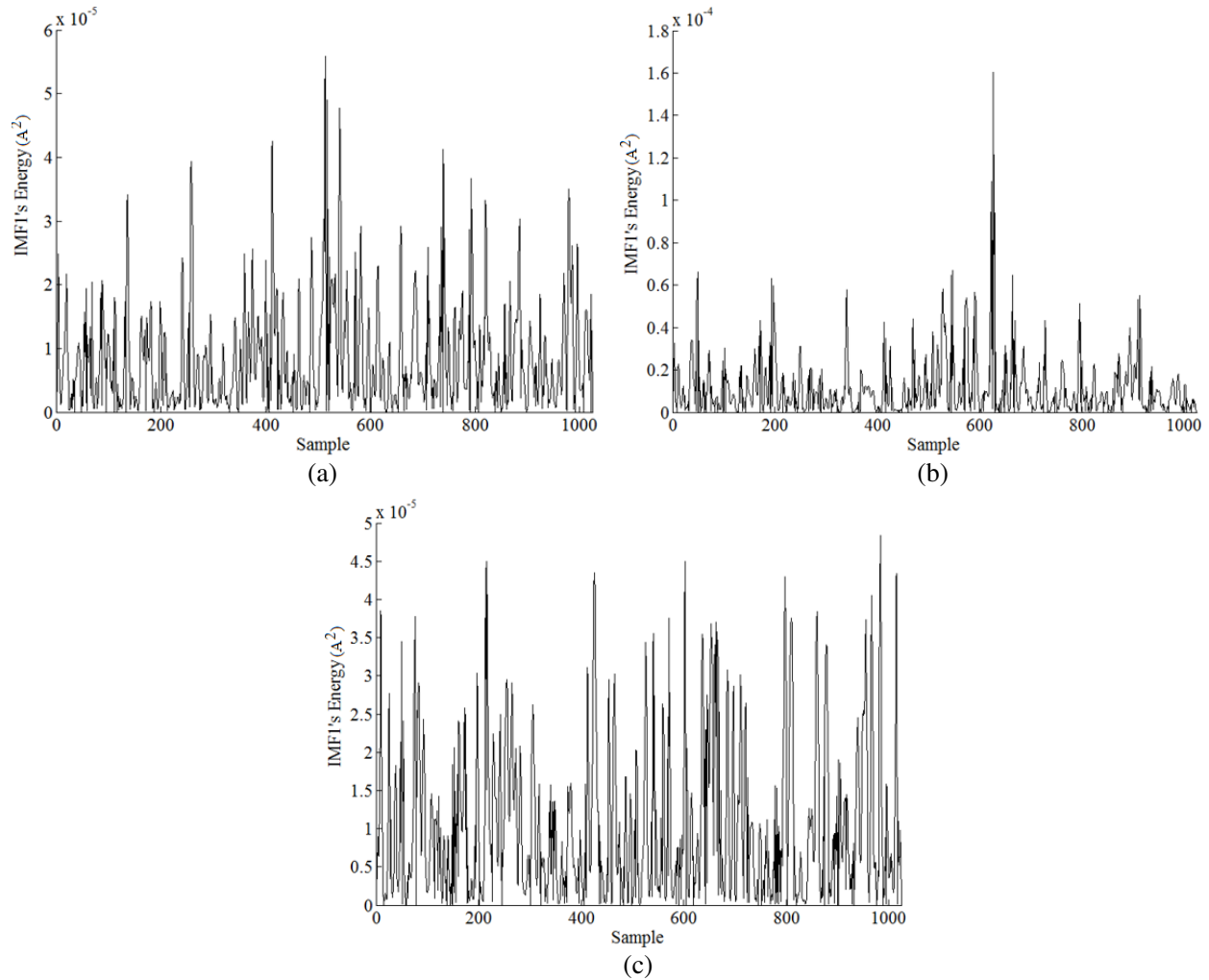


Figure 9. Energy of first intrinsic mode functions. (a) Ash tree (Sample 1). (b) Cherry tree (Sample 1). (c) Walnut tree (Sample 1).

was extracted employing EMD. The first and second IMFs obtained from decomposition were chosen for evaluation.

Figures 9 and 10 show the energy of the first and second IMFs for the first sample of cherry, walnut, and ash tree. As evident in these figures, none of the functions have the same distribution. Pulse peak values are also not the same, and there is no apparent relationship between IMFs. In other words, data related to IMFs were not actually distributed according to a given distribution and had a lot of outliers that were far removed from the mean. Therefore, finding a relationship between them was not possible at this stage, and other tools had to be employed. That is why QR method was chosen to find the relationship between energys of IMFs obtained from EMD of THIF. Indeed, the QR method was employed to predict expected behavior of a THIF. This method is a powerful tool for real-time detection of abnormality in which it could capture the extreme values in data distribution of each IMF.

Q-quantiles are values that divide the group of discrete energy coefficients into q subsets of same sizes so that there are $q - 1$ of the q -quantiles. The q -quantiles are the results of applying the inverse function of the cumulative distribution function to the values of $\{\frac{1}{q}, \frac{2}{q}, \dots, \frac{q-1}{q}\}$.

In order to extract the feature contained within energy coefficients of first and second IMFs of THIFs, specific trend between quantiles of these coefficients for different sample of THIFs and other disturbed signals was taken into consideration, and according to the results of conducted evaluations, the following algorithm for THIF detection was extracted:

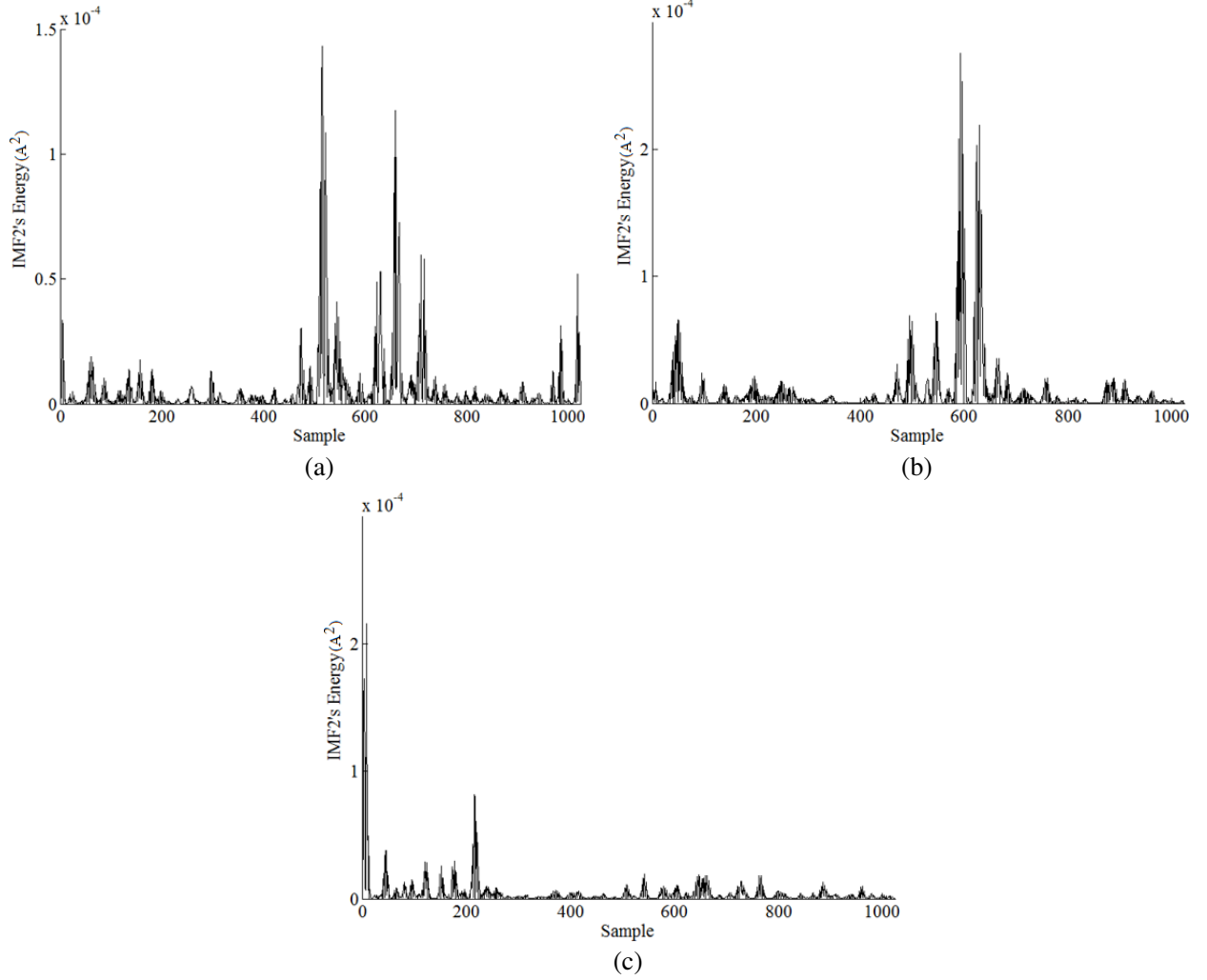


Figure 10. Energy of second intrinsic mode functions. (a) Ash tree (Sample 1). (b) Cherry tree (Sample 1). (c) Walnut tree (Sample 1).

1. Modeled THIF signal is decomposed according to the EMD algorithm [8].
2. Intrinsic mode functions of first and second are extracted.
3. Energy coefficients of each IMF are calculated.
4. The values of energy coefficients of each IMF are considered as a population.
5. Quantiles of each population are calculated according to the flowchart in Fig. 11.
6. The set of intervals for the calculated quantiles is chosen.
7. Quantiles of IMF₂ distribution are plotted against the same quantiles of IMF₁ distribution in separate plots.
8. Linear regression between the quantiles is estimated.
9. The slope of estimated lines is calculated.
10. If the following conditions are met, the captured signal belongs to tree-related HIF:
 - The slope of the linear regression between the quantiles is between 0.2 and 0.5.
 - Most of the points follow a linear pattern.
 - A few outliers are evident at the central part of the range in quantiles-quantiles (Q-Q) plot.
 - The outliers depart upward from the straight line as you follow the quantiles from left to right.

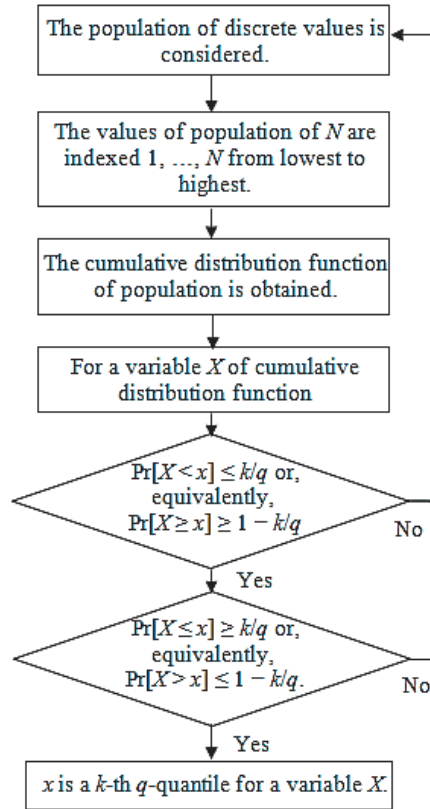


Figure 11. Algorithm of Quantiles calculation of each population.

6. RESULTS AND DISCUSSION

The results of application of suggested algorithm to energy coefficients of different THIFs are summarized as a series of scatterplots created by plotting two sets of quantiles related to energy of the first and second IMFs against one another (Fig. 12). These quantiles are the points in data below which a certain proportion of data fall and therefore can be utilized as an efficient index in detection targets. Superimposed on the plots are the lines joining the first and third quartiles of each distribution. These are the robust linear fits of the order statistics of the two distribution of energy of the first and second IMFs. These lines are extrapolated out to the ends of the sets and represent the specific trend between energy of first and second IMFs. So, the slope of these lines indicates a specific feature of THIF.

As evident in scatterplots of Fig. 12, most of the data follow a linear pattern and are distributed on the left side with a short tail of data extending out to the right. However, a few outliers being evident at the central part of the range reveal that some data of the first and second IMFs are not distributed in the same manner. The points depart upward from the straight line as you follow the quantiles from left to right. The straight line illustrates where the points would fall if the IMF2’s energy dataset was perfectly distributed, the same as IMF2’s energy dataset. The point’s upward trend demonstrates that the value of IMF2’s energy quantiles is much greater than the value of IMF1’s energy quantiles.

According to the proposed algorithm, the expected range for the first THIF criterion is 0.2–0.5. As evident in Table 4, the values of this criterion are all between 0.2 and 0.5. Given that all the conditions stated in the algorithm have been met for all samples, THIF was accurately detected.

In order to validate the specificity of suggested technique, the QR method was also applied to other disturbed signals generated by different power-electronic converters. These signals generated under normal conditions of power system may lead to the misoperation of THIF detectors [25]. Fig. 13 shows four samples of these signals.

As shown in scatterplots of Fig. 14, Q-Q plots of disturbed signals do not show the same trend

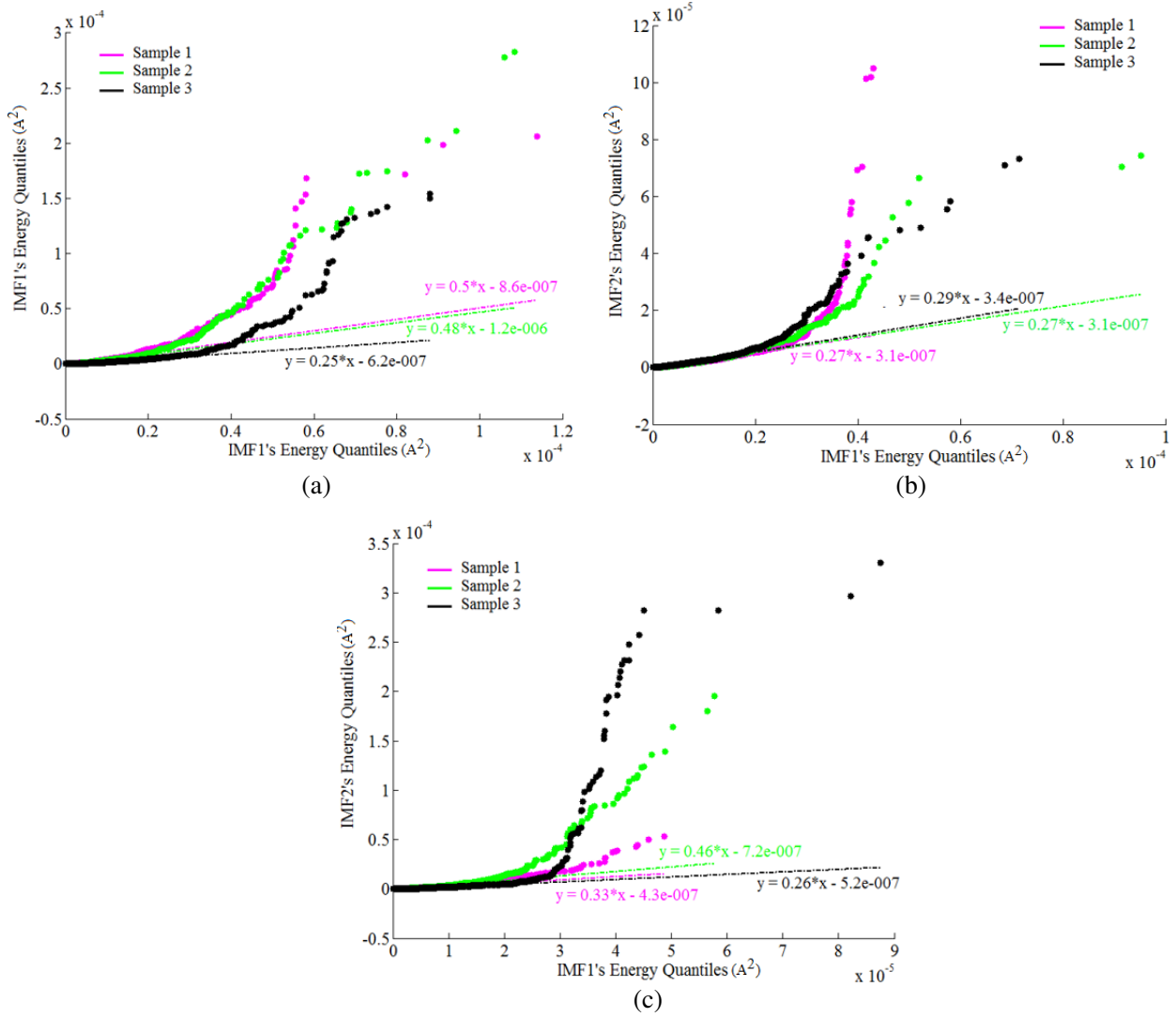


Figure 12. The quantile regression results for tree-related HIFs. (a) Cherry tree. (b) Walnut tree. (c) Ash tree.

Table 4. Slope of the linear regressions for all THIF tests.

Type of Tree Based on Vascular Structure	Tested Tree Species	Sample Tree Number	Criterion Value	Criterion Range for Tree-related HIF	Tree-related HIF Feature
Diffuse Porous	Cherry	1	0.5	0.2–0.5	✓
		2	0.48		✓
		3	0.25		✓
Semi-ring Porous	Walnut	1	0.27		✓
		2	0.27		✓
		3	0.29		✓
Ring Porous	Ash	1	0.33		✓
		2	0.46		✓
		3	0.26		✓

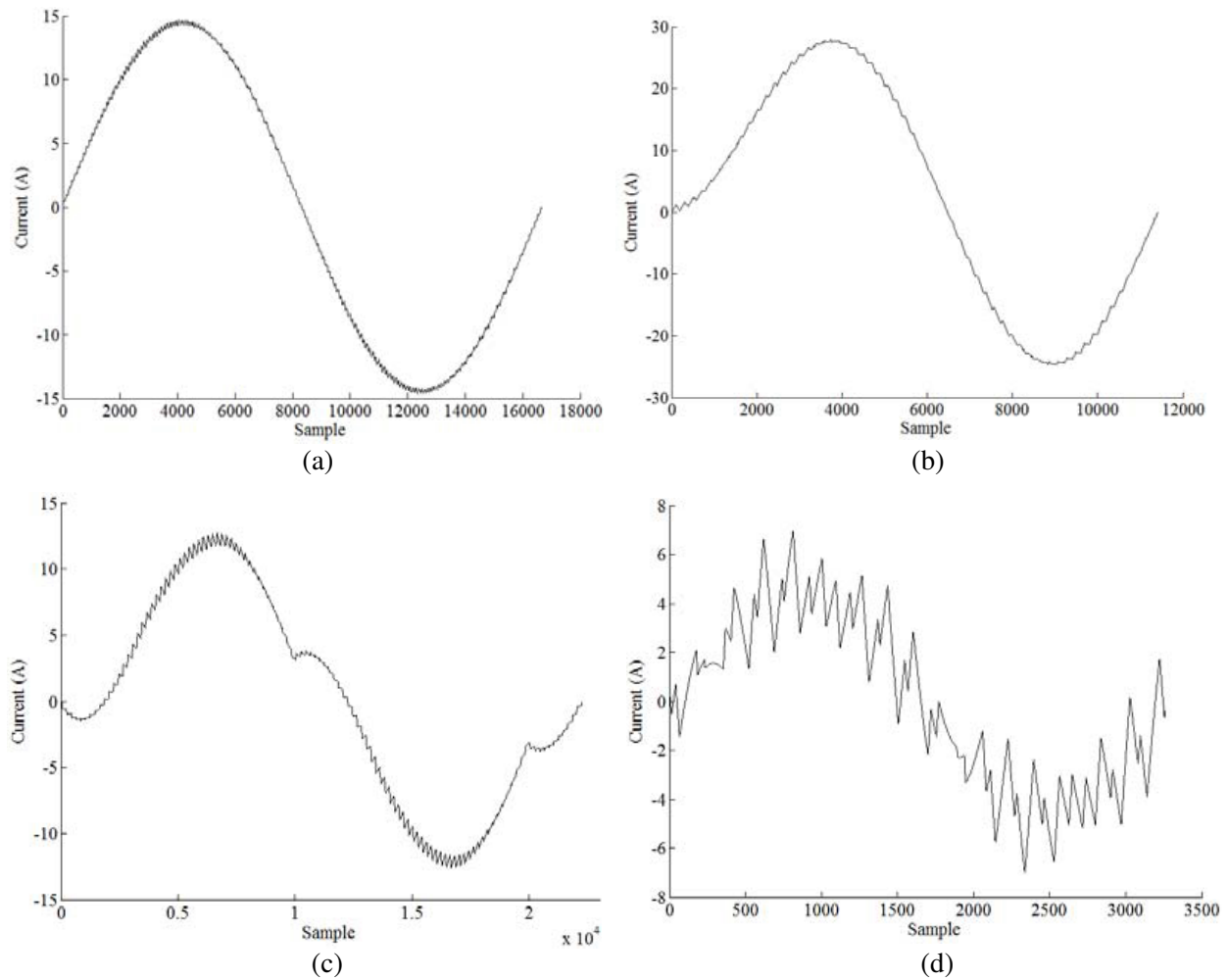


Figure 13. Signals generated by power-electronic converters. (a) Current signal generated by 3-phase bipolar inverter. (b) Current signal generated by 3-phase unipolar inverter. (c) Current signal generated by 3-phase SPWM inverter. (d) Current signal generated by 3-phase voltage source converter (VSC).

Table 5. Slope of the linear regressions for disturbed signals.

Disturbed signal other than the tree-related HIF	Criteria Value	Criteria Range for THIF	THIF Feature
Disturbed current signal generated by 3-phase bipolar inverter	0.13	0.2–0.5	×
Disturbed current signal generated by 3-phase unipolar inverter	0.053		×
Disturbed current signal generated by 3-phase SPWM inverter	4.4		×
Disturbed current signal generated by 3-phase VSC	1.1		×

observed in THIF. In all Q-Q plots of disturbed signals, there are more outliers to the left of the IMF1’s distribution compared to THIF’s Q-Q plots, so it could not be concluded that most of the points follow a linear pattern. The slopes of straight lines in all plots are not in the expected range for the first THIF criterion. The outliers cross the straight line of the Q-Q plot in Fig. 14(c). In Fig. 14(c) and Fig. 14(d),

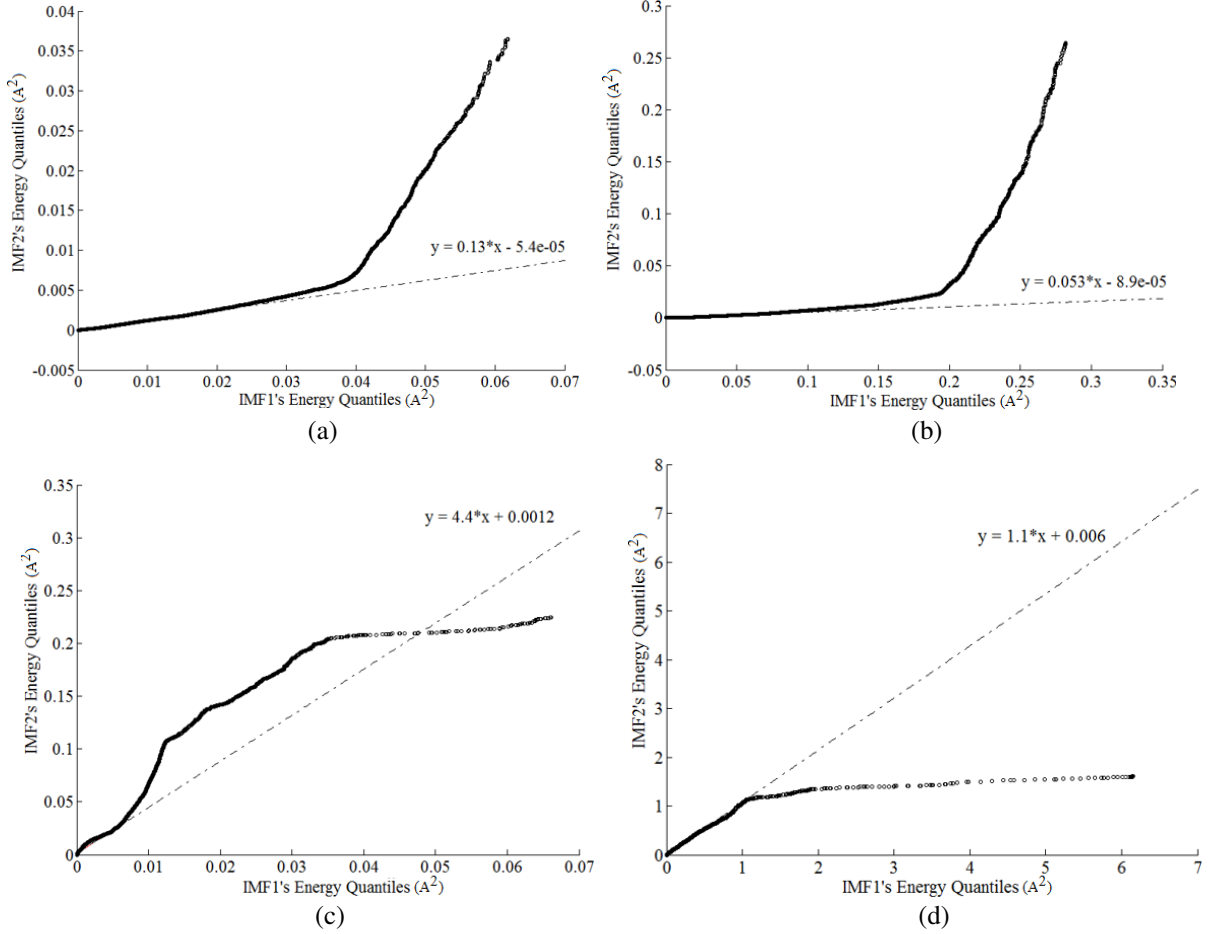


Figure 14. The quantile regression results for disturbed signals. (a) Current signal generated by 3-phase bipolar inverter. (b) Current signal generated by 3-phase unipolar inverter. (c) Current signal generated by 3-phase SPWM inverter. (d) Current signal generated by 3-phase VSC.

the outliers appear below the straight line because those quantiles occur at much lower values than where those quantiles would be in an IMF1's energy distribution.

As evident in Table 5, the slope of the linear regressions for the evaluated disturbed signals are out of expected range. Given that all the conditions mentioned in the proposed algorithm have not been met for evaluated disturbed signals, these signals are not detected as tree-related HIF.

In summary, the extracted features for tree-related HIF according to results obtained are as follows:

- 1- The slope of the linear regression between the quantiles is between 0.2 and 0.5.
- 2- Most of the points follow a linear pattern.
- 3- A few outliers are evident at the central part of the range in quantiles-quantiles plot.
- 4- The outliers depart upward from the straight line as you follow the quantiles from left to right.

7. CONCLUSION

In this paper, besides proving the ability of THIF in generating electromagnetic noise, a hybrid THIF detection approach based on the statistical method was proposed. To achieve this, the real THIF signal was first analyzed employing the FEM, and then an applicable index was extracted for THIF detection based on the statistical relations between the energy of IMFs obtained from EMD. Indeed, what can be considered as a criteria for THIF detection in the proposed method was the specific trend between the energy of first and second IMFs. The validation of the proposed method was determined by comparing the QR results obtained from the different samples of THIF signal with those obtained from other disturbed signals.

This proposed method could help in identifying the potential areas of EMI due to the THIFs as quickly as possible without the burden of expensive test equipment and setups. Once the source is identified, the experts could begin to build up a list of solutions to the problems.

This technique could be practically applied in two ways: 1. using the magnetic field detector which picks up the electromagnetic waves emanating from THIFs. As noted, the THIF can generate electromagnetic waves with HF components on the surrounding power lines which are approximately proportional to the power line's currents. Sensitive measurement can be achieved using built-in HF antennas/sensors or external antennas/sensors mounted on insulating spacers in the surrounding power lines. These antennas/sensors could detect magnetic fields with resolution of micro tesla. 2. Using electrical current detector which picks up the three-phase current signals of power lines using HF current transformers placed at the sending end of the feeders.

Other results obtained from this research include:

1. EMD is a capable technique for components decomposition of HIF signals.
2. High frequency magnetic fields generated by tree-related HIF are one of the sources of EMI.

ACKNOWLEDGMENT

The author wishes to thank Electricity Distribution Company of Hamedan for their participation in data collection.

REFERENCES

1. Campi, T., S. Cruciani, V. De Santis, F. Palandrani, F. Maradei, and M. Feliziani, "Induced effects in a pacemaker equipped with a wireless power transfer charging system," *IEEE Trans. Magn.*, Vol. PP, No. 99, 1–1, Jan. 2017.
2. Sun, H., X. Cui, and L. Du, "Electromagnetic interference prediction of ± 800 kV UHVDC converter station," *IEEE Trans. Magn.*, Vol. 52, No. 3, Mar. 2016.
3. Yang, Z., H. Li, F. Lin, B. Zhang, and J. Lü, "Common-mode electromagnetic interference calculation method for a PV inverter with chaotic SPWM," *IEEE Trans. Magn.*, Vol. 51, No. 11, Nov. 2015.
4. Chen, H., H. H.-C. Iu, and Y. Zhao, "Economic integration based solution for EMI noise in switched reluctance motor drive," *IEEE Trans. Magn.*, Vol. 48, No. 2, 859–862, Feb. 2012.
5. Ranjith Kumar, V. S. N., S. Kumar, G. Pal, and T. Shah, "High-ampacity overhead power lines with carbon nanostructure — Epoxy composites," *J. Eng. Mater. Technol.*, Vol. 138, No. 4, Jun. 2016.
6. Pous, M. and F. Silva, "Full-spectrum APD measurement of transient interferences in time domain," *IEEE Trans. Electromagn. Compat.*, Vol. 56, No. 6, 1352–1360, Dec. 2014.
7. Pous, M. and F. Silva, "Prediction of the impact of transient disturbances in real-time digital wireless communication systems," *IEEE Electromagn. Compat. Mag.*, Vol. 3, No. 3, 76–83, Jul./Sep. 2014.
8. Azpurua, M. A., M. Pous, and F. Silva, "On the statistical properties of the peak detection for time-domain EMI measurements," *IEEE Trans. Electromagn. Compat.*, Vol. 57, No. 6, 1374–1381, Dec. 2015.
9. Xiao, C. and T. Zhao, "Identification method of EMI sources based on measured single-channel signal and its application in aviation secondary power source design," *IEEE Trans. Electromagn. Compat.*, Vol. PP, No. 99, 1–8, Oct. 2016.
10. Ghaderi, A., H. Mohammadpour, H. Ginn, III, and Y. Shin, "High impedance fault detection in distribution network using time-frequency based algorithm," *IEEE Trans. Power Deliv.*, Vol. 99, PP, 2014.
11. Macedo, J. R., J. W. Resende, C. A. Bissochi, D. Carvalho, and F. C. Castro, "Proposition of aninterharmonic-based methodology for high-impedance fault detection in distribution systems," *IET Gener. Transm. Distrib.*, Vol. 9, No. 16, 2593–2601, 2015.

12. Iurinic, L. U., A. R. Herrera-orozco, R. G. Ferraz, and A. S. Bretas, "Distribution systems high-impedance fault location: A parameter estimation approach," *IEEE Trans. Power Deliv.*, Vol. 31, 1806–1814, 2016.
13. Elkalashy, N. I., M. Lehtonen, H. A. Darwish, M. A. Izzularab, and A. M. I. Taalab, "Modeling and experimental verification of high impedance arcing fault in medium voltage networks," *IEEE Trans. Dielectr. Electr. Insul.*, Vol. 14, 375–383, 2007.
14. Maximov, V. T. H. F. R. S. and J. L. Guardado, "High impedance fault location formulation: A least square estimator based approach," *Math. Problems Eng.*, 1–10, 2014.
15. Costa dos Santos, W., B. Alencar de Souza, N. Silva Dantas Brito, F. Bezerra Costa, and M. Renato Cerqueira Paes, Jr., "High impedance faults: From field tests to modeling," *Journal of Control, Automation and Electrical Systems*, Vol. 24, No. 6, 885–896, Sep. 2013.
16. Mahari, A. and H. Seyedi, "High impedance fault protection in transmission lines using a WPT-based algorithm," *Int. J. Electr. Power Energy Syst.*, Vol. 67, 537–545, 2015.
17. Biradar, P. and V. R. Sheelvant, "High-impedance fault detection using wavelet transform," *Int. J. Eng. Res. Gen. Sci.*, 166–173, 2015.
18. Azpúrua, M. A., M. Pous, and F. Silva, "Decomposition of electromagnetic interferences in the time-domain," *IEEE Trans. Electromagn. Compat.*, Vol. 58, No. 2, 385–392, Apr. 2016.
19. Chan, J. C., H. Ma, and T. K. Saha, "Self-adaptive partial discharge signal de-noising based on ensemble empirical mode decomposition and automatic morphological thresholding," *IEEE Trans. Dielectr. Electr. Insul.*, Vol. 21, 294–303, 2014.
20. Zhang, H., T. R. Blackburn, and B. T. Phung, "A novel wavelet transform technique for on-line partial discharge measurements. 1. WT de-noising algorithm," *IEEE Trans. Dielectr. Electr. Insul.*, Vol. 14, 2007.
21. Hacke, U. G. and J. S. Sperry, "Functional and ecological xylem anatomy," *Perspectives in Plant Ecology, Evolution and Systematics 4: Science Direct*, 97–115, 2001.
22. Evert, R. F., *Esau's Plant Anatomy: Meristems, Cells, and Tissues of the Plant Body: Their Structure, Function, and Development*, 3rd Edition, Published Online: 6, Feb. 2006.
23. Bittner, S., M. Janott, D. Ritter, P. Köcher, F. Beese, and E. Priesack, "Functional-structural water flow model reveals differences between diffuse- and ring-porous tree species," *Agricultural and Forest Meteorology*, Vol. 158–159, 80–89, 2012.
24. ETSI EN 302 608 V1.1.1, European Telecommunications Standards Institute, 2007.
25. Ghaderi, A., H. A. Mohammadpour, H. L. Ginn, and Y. Shin, "High-impedance fault detection in the distribution network using the time-frequency-based algorithm," *IEEE Trans. Power Deliv.*, Vol. 30, No. 3, 1260–1268, 2015.